

# DETERMINATION OF THE FRACTURE INITIATION IN DUCTILE MATERIAL, BASED ON GURSON'S MODEL COUPLED WITH SHEAR MECHANISMS

Natália S. I. Aoyama, natalia\_seyko@aluno.unb.br

Lucival Malcher, malcher@unb.br

João V. Sahadi, joao\_sahadi@aluno.unb.br

Raniere S. Neves, raniere\_neves@aluno.unb.br

UnB – University of Brasília, Faculty UnB Gama, Distrito Federal - Brazil

Fábio J. P. Reis, fabio.reis@fe.up.pt

Thiago Doca, thiago.doca@fe.up.pt

Filipe X. C. Andrade, filipe.xavier@fe.up.pt

IDMEC – Institute of Mechanical Engineering, Faculty of Engineering, University of Porto, Porto, Portugal.

**Abstract.** *In this paper, it is focusing the evaluation of two shear mechanisms proposed by Xue and Nahshon and co-authors, and coupled in the damage variable of the Gurson-Tvergaard-Needleman model (GTN). Initially, a brief summary of the GTN's model is performance as well as both shear mechanisms. After that, an implicit numerical integration algorithm, based on the operator split methodology, is implemented in an "in house" academic finite element environment. Besides that, the so called "butterfly specimen" is used, and the material properties of an aluminum alloy 2024-T351. Regarding the numerical simulations, the performance of both shear mechanisms is evaluated based on the evolution of the equivalent plastic strain and damage variable at the critical point of the specimen. The ability to predict the correct fracture location is also investigated, mainly when low levels of stress triaxiality is presented. At the end, the best performance of the model is highlighted, when predominant shear loading condition is presented, based on the agreement between experimental and numerical data.*

**Keywords:** *shear mechanism, Gurson's model, fracture location.*

## 1. INTRODUCTION

The fracture in metals is an important subject to be improved, regarding the ability to predict the correct location of crack initiation in machine components and rupture in general structures. This phenomenon can be studied by its separated evolution contribution as the initiation and growth of general micro defects which is induced by large deformations. Some researchers like McClintock (1968) and Rice & Tracey (1969) developed pioneering work undertaken on the subject, where the nature of defect was taken into account the study of ductile damage by analyzing its geometry in a continuous matrix.

The degradation of material properties is an irreversible process and starts from the formation of micro defects which can be voids, cracks and others, that already exist or that will be formed in the material matrix. However, the evolution of material degradation is dependent on macroscopic loading conditions which can cause a volumetric void growth such as in tensile loading condition or a preferential elongation of micro defects which can be observed in pure shear loading conditions. The ductile fracture phenomenon can be described, based on a micromechanical analysis of micro cavity growth, especially for the fracture computation within local approaches of fracture, (see Pineau, 1981; Rousselier, 1987; Besson et al., 2001) or based on the Continuum Damage Mechanics theory and a thermodynamic framework, either phenomenological or micromechanically based, as Lemaitre (1985) for damage caused by plastic flow, Chaboche (1984) and Murakami & Ohno (1981) for creep damage, Krajčinović & Fonseka (1981) on micromechanical grounds.

The formulations proposed by Lemaitre and Gurson are the most important coupled damage ductile models to describe the above two methodologies (see Chaboche et al., 2006). Since then, motivated by the limitations of these classical models, such as in prediction of the correct fracture location or in determination of the correct values of the internal variables at fracture, many researchers have proposed improvements in both methodologies, by introducing more effects in the constitutive formulation or in the damage evolution law like the pressure effect, temperature, Lode angle dependence, viscoplastic effects, crack closure effect, shear mechanisms, among others (Tvergaard & Needleman, 1984; Rousselier, 1980 and 2001; Xue, 2007; Nahshon & Hutchinson, 2008; Lemaitre & Chaboche, 1990; Chaboche, 2003; Andrade Pires et al., 2003; Chaboche et al., 2006; Besson, 2010).

These classical coupled damage models have the ability to predict the correct fracture location under a specific range of stress triaxialities (see Xue, 2007; Nahshon et al.; 2008; Teng, 2008) and are extremely accurate for loading conditions close to the calibration point (see Malcher, 2011). For example, within range of high levels of stress triaxialities, where the spherical void growth is the predominant mechanism, the models based on Gurson theory, like the Gurson-Tvergaard-Needleman model (GTN), have good performance in prediction of fracture location and

parameters in fracture as equivalent plastic strain and displacement. However, under shear dominated loads, where failure is mainly driven by the shear localization of plastic strain of the inter-voids ligaments due to void rotation and distortion, the model does not perform well, (see Engelen, 2005; Chaboche, 2006). Figure 1 illustrates the ductile failure mechanism, which can occur by internal necking (Figure 1a), where the large primary voids are formed due to high stress triaxiality and the inter ligaments are done mainly by a sharp volumetric or by void sheeting (Figure 1b), where primary voids remain small due to low stress triaxiality and the inter ligament occurs by mainly elongation of voids and formation of secondary voids in strain localization bands.

Due to these two types of ductile failure mechanisms, it is expected that the population of micro defects, that can be nucleated, would be higher in void sheeting than in internal necking.

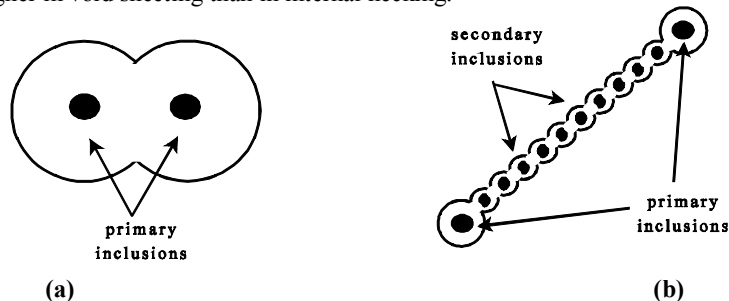


Figure 1. Schematic representation of ductile failure mechanism (a) internal necking and (b) void sheeting. Adapted from Besson, (2010).

## 2. CONSTITUTIVE FORMULATION AND NUMERICAL INTEGRATION ALGORITHM

Inspired by the work of Gurson (1977), Tvergaard and Needleman (1984) have proposed a model for the description of damage and fracture in ductile materials. The original Gurson model introduces a strong coupling between plastic strain and damage (Chaboche *et al.*, 2006) and the presence of micro voids in the formulation leads to a yield surface that depends on both the hydrostatic pressure and porosity. The material degradation is measured through a parameter called the void volume fraction, which is represented by the variable  $f$ . This parameter is defined by the ratio between the volume of micro voids,  $V_{voids}$ , and the representative volume element,  $V_{RVE}$ .

$$f = \frac{V_{voids}}{V_{RVE}} \quad (1)$$

The Gurson-Tvergaard-Needleman (GTN) model, which is one of the most well known extensions of Gurson's model, assumes both isotropic hardening and damage. Nevertheless, the damage variable in this model is represented by an effective porosity  $f^*$ . The flow potential is generalized into the form:

$$\Phi(\sigma, r, f^*) = J_2(\mathbf{S}) - \frac{1}{3} \left\{ 1 + q_3 \cdot f^{*2} - 2 \cdot q_1 \cdot f^* \cdot \cosh\left(\frac{q_2 \cdot 3 \cdot p}{2 \cdot \sigma_y}\right) \right\} \cdot \sigma_y^2 \quad (2)$$

where,  $J_2$  represents the second invariant of the deviatoric stress tensor and  $\sigma_y$  is the isotropic hardening law. The parameters  $q_1$ ,  $q_2$  and  $q_3$  are introduced into the yield surface definition in order to bring the model predictions into closer agreement with full numerical analyses of a periodic array of voids and  $p$  represents the hydrostatic pressure. The evolution of spherical voids can be reproduced by three simultaneous or successive steps: nucleation, growth and coalescence of voids (Tvergaard & Needleman, 1984). The effective porosity is determined by the following bilinear function:

$$f^* = \begin{cases} f & , \quad f < f_c \\ f_c + \left(\frac{1}{q_1} - f_c\right) \frac{(f - f_c)}{(f_f - f_c)} & , \quad f \geq f_c \end{cases} \quad (3)$$

where, the parameter  $f$  represents the porosity, the constant  $f_c$  is the porosity to trigger coalescence and the parameter  $f_f$  represents the porosity at fracture. The evolution of the porosity is given by the sum of both the nucleation and growth mechanisms, as:

$$\dot{f} = \dot{f}^N + \dot{f}^G \quad (4)$$

The nucleation mechanism is driven by the plastic strain and can be represented as:

$$\dot{f}^N = \frac{f_N}{s_N \cdot \sqrt{2\pi}} \cdot \exp \left[ -\frac{1}{2} \left( \frac{\bar{\varepsilon}^p - \varepsilon_N}{s_N} \right)^2 \right] \dot{\bar{\varepsilon}}^p \quad (5)$$

where,  $f_N$  represents the volume fraction of all second-phase particles (see Figure 1b) with potential for micro void nucleation,  $\varepsilon_N$  and  $s_N$  are the mean strain for void nucleation and its standard deviation. The variable  $\bar{\varepsilon}^p$  represents the equivalent plastic strain and  $\dot{\bar{\varepsilon}}^p$  is the rate of the equivalent plastic strain.

The most significant contribution to the evolution of spherical voids is the growth mechanism, which is obtained from the condition of plastic incompressibility of the matrix material, can be expressed by:

$$\dot{f}^G = (1 - f) \text{tr}(\dot{\boldsymbol{\varepsilon}}^p) = (1 - f) \cdot \dot{\varepsilon}_v^p \quad (6)$$

where,  $\dot{\boldsymbol{\varepsilon}}^p$  represents the rate of the plastic strain tensor and  $\dot{\varepsilon}_v^p$  is the rate of the volumetric plastic strain. In this work, the GTN's model implementation includes both nucleation and growth of micro voids. The coalescence effect of was not addressed since our main objective is the prediction of damage onset.

## 2.1. Shear mechanism

Regarding the limitation of the Gurson original model in prediction failure when void sheeting mechanism plays the main role, researchers as Xue (2007), Nahshon & Hutchinson (2008), Butcher et al. (2009) have suggested the introduction of another mechanism as shear, in the evolution law of the Gurson's damage parameter. Both researchers have initially formulated shear mechanisms based on phenomenological and geometrical aspects resulting in expression dependent on the equivalent strain and its rate and a Lode angle function. Xue (2008), based on the volume conservation of a cubic cell, has proposed that the rate of the shear damage can be written by:

$$\dot{D}_{shear} = q_4 \cdot g_0 \cdot f^{q_5} \cdot \varepsilon_{eq} \cdot \dot{\varepsilon}_{eq} \quad (7)$$

where,  $q_4$  and  $q_5$  are geometrical parameters and can be defined according to two or three dimensional problem. For two dimensional problem,  $q_4 = \frac{3}{\sqrt{\pi}}$  and  $q_5 = (1/2)$  and for three dimensional problem,  $q_4 = \frac{3}{2} \left( \frac{6}{\pi} \right)^{(1/3)}$  and  $q_5 = (1/3)$ .  $\varepsilon_{eq}$  and  $\dot{\varepsilon}_{eq}$  represent the equivalent strain and its rate, respectively.  $g_0$  denotes the Lode angle function that by Xue is defined as:

$$g_0 = (1 - |\bar{\theta}|) \quad (8)$$

where,  $\bar{\theta}$  is the normalized Lode angle, which can be expressed as  $\bar{\theta} = 1 - \frac{2}{\pi} \text{acos}(\xi)$  and  $\xi$  is the normalized third invariant, which is a ratio between the third invariant of the deviatoric stress tensor,  $r = [(27/2) \cdot \det \mathbf{S}]^{1/3}$ , and the von Mises equivalent stress,  $q = \sqrt{(3/2) \mathbf{S} : \mathbf{S}}$ .

Nahshon & Hutchinson (N&H) have suggested a shear mechanism based on phenomenological aspects that can be written as (see Nahshon et al, 2008):

$$\dot{D}_{shear} = k \cdot f \cdot g_0 \cdot \frac{\mathbf{S} : \boldsymbol{\varepsilon}^p}{q} \quad (9)$$

where,  $k$  is a material parameter and needs to be calibrated.  $\boldsymbol{\varepsilon}^p$  denotes the plastic strain tensor. The Lode angle function by Nahshon et al. (2008) is defined as:

$$g_0 = (1 - \xi^2) \quad (10)$$

Thus, the damage internal variable rate (Equation 4) can be re-written according to Equation 11.

$$\dot{f} = \dot{f}^n + \dot{f}^g + \dot{D}_{shear} \quad (11)$$

**Box 1.** GTN's model including nucleation, growth of micro voids and shear mechanisms.

(i) Elasto-plastic split of the strain tensor

$$\boldsymbol{\varepsilon} = \boldsymbol{\varepsilon}^e + \boldsymbol{\varepsilon}^p$$

(ii) Elastic law

$$\boldsymbol{\sigma} = \mathbf{D}^e : \boldsymbol{\varepsilon}^e$$

(iii) Yield function

$$\Phi(\boldsymbol{\sigma}, r, f) = J_2(\mathbf{S}) - \frac{1}{3} \left\{ 1 + q_3 \cdot f^2 - 2 \cdot q_1 \cdot f \cdot \cosh\left(\frac{q_2 \cdot 3 \cdot p}{2 \cdot \sigma_y}\right) \right\} \cdot \sigma_y^2$$

(iv) Plastic flow and evolution equations for  $r$  and  $f$

$$\dot{\boldsymbol{\varepsilon}}^p = \dot{\gamma} \cdot \left[ \mathbf{S} + \frac{1}{3} q_1 \cdot q_2 \cdot f \cdot \sigma_y \cdot \sinh\left(\frac{q_2 \cdot 3 \cdot p}{2 \cdot \sigma_y}\right) \cdot \mathbf{I} \right]$$

$$\dot{r} = \dot{\gamma} \cdot \frac{\left\{ q_1 \cdot q_2 \cdot f \cdot p \cdot \sinh\left(\frac{q_2 \cdot 3 \cdot p}{2 \cdot \sigma_y}\right) + \frac{2}{3} \left[ 1 + q_3 \cdot f^2 - 2 \cdot q_1 \cdot f \cdot \cosh\left(\frac{q_2 \cdot 3 \cdot p}{2 \cdot \sigma_y}\right) \right] \cdot \sigma_y \right\}}{(1 - f)}$$

$$\dot{f} = \dot{f}^N + \dot{f}^G + \dot{f}^{Shear} = \frac{f_N}{s_N \cdot \sqrt{2\pi}} \cdot \exp\left[-\frac{1}{2} \left(\frac{\bar{\boldsymbol{\varepsilon}}^p - \varepsilon_N}{s_N}\right)^2\right] \frac{\dot{\boldsymbol{\varepsilon}}^p}{\bar{\boldsymbol{\varepsilon}}} + (1 - f) \cdot \dot{\varepsilon}_v^p + \dot{D}_{shear}$$

where,

$$\dot{D}_{shear} = \begin{cases} q_4 \cdot g_0 \cdot f^{q_5} \cdot \varepsilon_{eq} \cdot \dot{\varepsilon}_{eq}, & \text{if Xue's shear mechanism is chosen} \\ k \cdot f \cdot g_0 \cdot \frac{\mathbf{S} : \boldsymbol{\varepsilon}^p}{q}, & \text{if Nahshon's shear mechanism is chosen} \end{cases}$$

and,

$$\frac{\dot{\boldsymbol{\varepsilon}}^p}{\bar{\boldsymbol{\varepsilon}}} = \dot{\gamma} \cdot \sqrt{\frac{2}{3} \left\{ \mathbf{S} : \mathbf{S} + \frac{1}{3} \left[ q_1 \cdot q_2 \cdot f \cdot \sigma_y \cdot \sinh\left(\frac{q_2 \cdot 3 \cdot p}{2 \cdot \sigma_y}\right) \right]^2 \right\}}$$

$$\dot{\varepsilon}_v^p = \dot{\gamma} \cdot q_1 \cdot q_2 \cdot f \cdot \sigma_y \cdot \sinh\left(\frac{q_2 \cdot 3 \cdot p}{2 \cdot \sigma_y}\right)$$

(v) Loading/unloading criterion

$$\dot{\gamma} \geq 0, \quad \Phi \leq 0, \quad \dot{\gamma} \Phi = 0.$$

## 2.2. Numerical integration algorithm

In this section, a numerical integration algorithm for GTN's modified model is taken, which was initially proposed by the authors. The algorithm was building, regarding an implicit solution and based on operator split methodology, which is especially suitable for the numerical integration of the evolution problem and have been widely used in computational plasticity (see Simo & Hughes, 1998; De Souza Neto *et al.*, 2008). This method, which is used here, consists of splitting the problem in two parts: an elastic predictor, where the problem is assumed to be elastic and, a plastic corrector, in which the system of residual equations comprising the elasticity law, plastic consistency and the rate equations is solved, taking the results of the elastic predictor stage as initial conditions. In the case of the yield condition has been violated, the plastic corrector stage is initiated and the Newton-Raphson procedure is used to solve the discretised equations. The Newton-Raphson procedure is chosen motivated by the quadratic rates of convergence achieved which results in return mapping procedures computationally efficient (see Simo & Hughes, 1998; De Souza Neto *et al.*, 2008). The overall algorithm for numerical integration is summarized in Box 2.

**Box 2.** Fully implicit Elastic predictor/Return mapping algorithm for GTN model with shear mechanism.

(i) Evaluate the elastic trial state: Given the incremental strain  $\Delta\varepsilon$  and the state variables at  $t_n$ :

$$\begin{aligned} \boldsymbol{\varepsilon}_{n+1}^{e\ trial} &= \boldsymbol{\varepsilon}_n^e + \Delta\boldsymbol{\varepsilon} & ; & \quad \bar{\varepsilon}_{n+1}^p\ trial = \bar{\varepsilon}_n^p & ; & \quad R_{n+1}^{trial} = R_n \\ f_{n+1}^{trial} &= f_n & ; & \quad \mathbf{S}_{n+1}^{trial} = 2G\boldsymbol{\varepsilon}_{n+1}^{e\ trial} & ; & \quad p_{n+1}^{trial} = K\varepsilon_{v\ n+1}^{e\ trial} \end{aligned}$$

(ii) Check plastic admissibility:

$$\text{IF } \Phi^{trial} = J_2^{trial} - \frac{1}{3} \left[ 1 + q_3 \cdot f_{n+1}^{trial\ 2} - 2 \cdot q_1 \cdot f_{n+1}^{trial} \cdot \cosh\left(\frac{3 \cdot q_2 \cdot p_{n+1}^{trial}}{2 \cdot \sigma_y}\right) \right] \cdot (\sigma_y^{trial})^2 \leq 0 \text{ THEN}$$

set  $(\cdot)_{n+1} = (\cdot)_{n+1}^{trial}$  (**elastic step**) and go to (v)

ELSE go to (iii)

(iii) Return mapping (**plastic step**): Solve the system of equations below for  $\Delta\gamma, p_{n+1}, f_{n+1}$  and  $R_{n+1}$ , using Newton-Raphson method.

$$\begin{cases} \frac{J_2^{trial}}{[1 + 2G \cdot \Delta\gamma]^2} - \frac{1}{3} \left[ 1 + q_3 \cdot f_{n+1}^2 - 2 \cdot q_1 \cdot f_{n+1} \cdot \cosh\left(\frac{3 \cdot q_2 \cdot p_{n+1}}{2 \cdot \sigma_y}\right) \right] \cdot \sigma_y^2 \\ p_{n+1} - p_{n+1}^{trial} + \Delta\gamma \cdot K \cdot \sigma_y \cdot q_1 \cdot q_2 \cdot f_{n+1} \cdot \sinh\left(\frac{3 \cdot q_2 \cdot p_{n+1}}{2 \cdot \sigma_y}\right) \\ f_{n+1} - f_{n+1}^{trial} - \frac{f_N}{S_N \sqrt{2 \cdot \pi}} \cdot \exp\left[-\frac{1}{2} \left(\frac{\bar{\varepsilon}_{n+1}^p - \varepsilon_N}{S_N}\right)^2\right] \cdot \Delta\bar{\varepsilon}^p - \Delta f^g - \Delta D_{shear} \\ R_{n+1} - R_{n+1}^{trial} - \Delta R \end{cases} = \begin{Bmatrix} 0 \\ 0 \\ 0 \\ 0 \end{Bmatrix}$$

where,

$$\Delta f^g = (1 - f_{n+1}) \cdot \Delta\gamma \cdot \sigma_y \cdot q_1 \cdot q_2 \cdot f_{n+1} \cdot \sinh\left(\frac{3 \cdot q_2 \cdot p_{n+1}}{2 \cdot \sigma_y}\right)$$

$$\Delta D_{shear} = \begin{cases} q_4 \cdot (1 - |\bar{\theta}_{n+1}^{trial}|) \cdot f_{n+1}^{q_5} \cdot \bar{\varepsilon}_{n+1}^p \cdot \Delta\bar{\varepsilon}^p, & \text{if Xue's mechanism} \\ k \cdot f_{n+1} \cdot (1 - \xi_{n+1}^{trial\ 2}) \cdot \Delta\bar{\varepsilon}^p, & \text{if Nahshon's mechanism} \end{cases}$$

$$\begin{aligned} \Delta R &= \frac{\Delta\gamma}{(1 - f_{n+1})} \cdot \left\{ q_1 \cdot q_2 \cdot f_{n+1} \cdot p_{n+1} \cdot \sinh\left(\frac{3 \cdot q_2 \cdot p_{n+1}}{2 \cdot \sigma_y}\right) \right. \\ &\quad \left. + \frac{2}{3} \cdot \sigma_y \cdot \left[ 1 + q_3 \cdot f_{n+1}^2 - 2 \cdot q_1 \cdot f_{n+1} \cdot \cosh\left(\frac{3 \cdot q_2 \cdot p_{n+1}}{2 \cdot \sigma_y}\right) \right] \right\} \end{aligned}$$

(iv) Update the others state variables:

$$\boldsymbol{\varepsilon}_{n+1}^e = \boldsymbol{\varepsilon}_{n+1}^{e\ trial} - \Delta\gamma \cdot \left[ \frac{\mathbf{S}_{n+1}^{trial}}{1 + 2G \cdot \Delta\gamma} + \frac{1}{3} \cdot \sigma_y \cdot q_1 \cdot q_2 \cdot f_{n+1} \cdot \sinh\left(\frac{3 \cdot q_2 \cdot p_{n+1}}{2 \cdot \sigma_y}\right) \cdot \mathbf{I} \right]$$

$$\mathbf{S}_{n+1} = \frac{\mathbf{S}_{n+1}^{trial}}{1 + 2G \cdot \Delta\gamma}$$

$$\bar{\varepsilon}_{n+1}^p = \bar{\varepsilon}_{n+1}^{p\ trial} + \Delta\gamma \cdot \sqrt{\frac{2}{3} \left\{ \frac{\mathbf{S}_{n+1}^{trial} : \mathbf{S}_{n+1}^{trial}}{1 + 2G \cdot \Delta\gamma} + \frac{1}{3} \left[ \sigma_y \cdot q_1 \cdot q_2 \cdot f_{n+1} \cdot \sinh\left(\frac{3 \cdot q_2 \cdot p_{n+1}}{2 \cdot \sigma_y}\right) \right]^2 \right\}}$$

(v) Exit

### 3. GEOMETRY, MESH DEFINITION AND CALIBRATION PROCEDURE

#### 3.1 Geometry and mesh definition

Regarding the material properties for the calibration point, a classical smooth bar specimen is used and Figure 2a presents the dimensions employed. In order to trigger necking, a dimensional reduction of 5% in the central diameter of the specimen is used. Besides that, based on the experimental data, a gauge section of 20.6 mm is also used. The

standard eight-noded axisymmetric quadrilateral element, with four Gauss integration points, is adopted. The initial mesh discretisation is illustrated in Figure 2b, where only one symmetric quarter of the problem, with the appropriate symmetric boundary conditions imposed to the relevant edges, is modelled. A total number of 1800 elements have been used in the discretisation of the smooth specimen, amounting to a total of 5581 nodes.

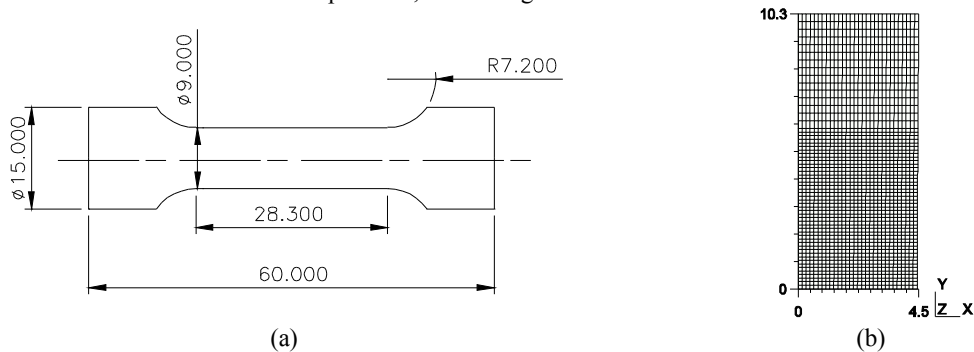


Figure 2. (a) The geometry for the smooth bar specimen. Dimension in (mm). Taken from Teng (2008). (b) Finite element mesh, regarding the gauge section of 20.6 mm.

According to the numerical simulation, a butterfly specimen is used. The specimen was initially designed by Bai (2008) and the geometry and general dimensions can be verified by Figure 3. In this case, a three dimensional finite element mesh of 2432 twenty noded elements, with nine Gauss integration points, is used amounting to 12681 nodes.

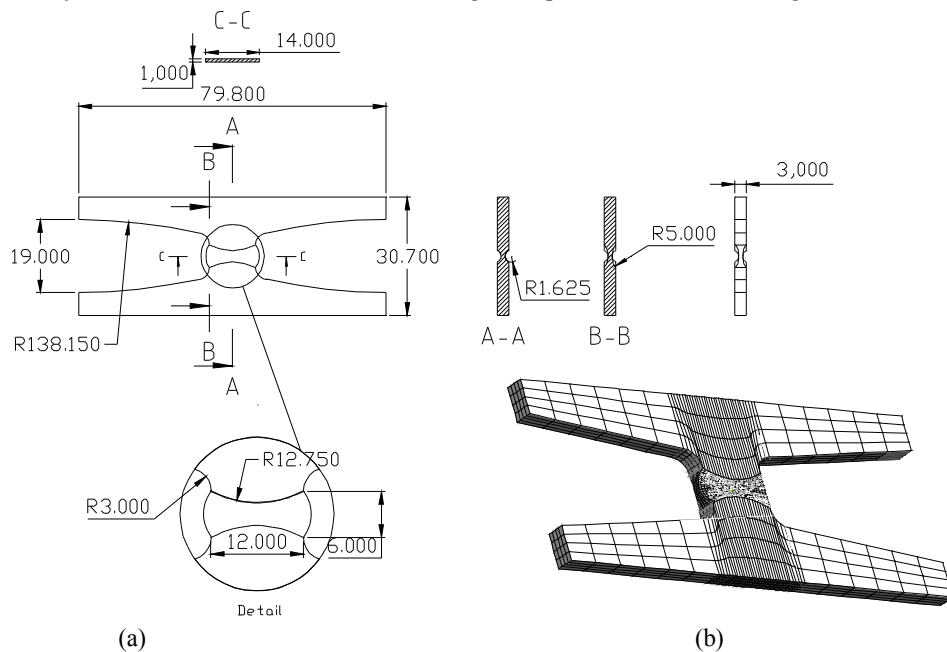


Figure 3. (a) The geometry for butterfly specimen. Dimension in (mm). Taken from Bai (2008). (b) Finite elements mesh for butterfly specimen.

### 3.2 Calibration procedure

In the present section the hardening law,  $\sigma_y(R)$ , for the undamaged model is determined as well as the set of parameters for nucleation of micro void mechanism  $[f_N, S_N, \epsilon_N]$  and the critical value for the damage variable,  $f_c$ . Through experimental tests conducted by Bai 2008, the reaction versus displacement curve is determined as well as the stress-strain curve for an elasto-plastic model of von Mises type. The inverse method is adopted in order to calibrate the material parameters for coupled damage model by forcing the numerical solution to be, as close as possible to the experimental results. Figure 4a shows the reaction curve for the model determined after the application of inverse method. A good agreement between the experimental and numerical results can be observed. Furthermore, the critical volume void fraction is also determined in the point where the model attains the displacement to fracture, experimentally observed (see Figure 4b). The critical value obtained is  $f_c = 0.076$ .

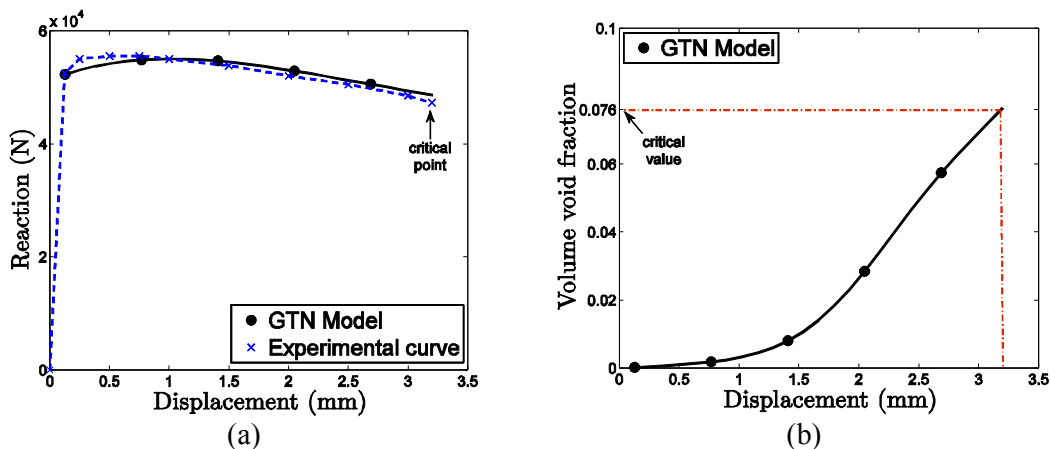


Figure 4. (a) Reaction versus displacement curve. (b) Critical volume voids fraction parameter

The results of the calibration procedure, in terms of stress-strain curve, can also be observed in Figure 5, where the curves, for uncoupled and coupled damage models, were determined.

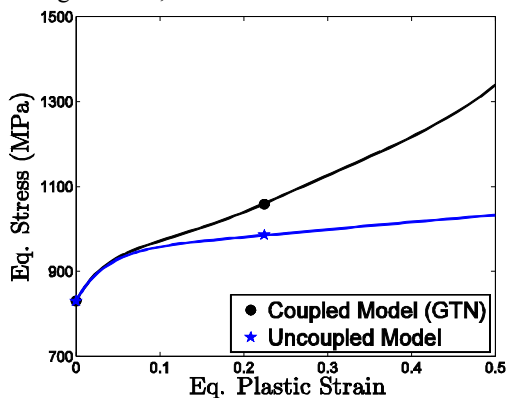


Figure 5. Stress-strain curves determined for an uncoupled and coupled models.

The material properties and others parameters related to the micro void nucleation mechanism obtained by employing an inverse method are listed in Table 1:

Table 1: Materials properties and parameters related to nucleation of micro-void mechanism for steel 1045.

Material	$f_N$	$S_N$	$\epsilon_N$	$q_1$	$q_2$	$q_3$	$f_c$	$E$ (MPa)	$\nu$
GTN	0.05	0.2	0.1	1.5	1.0	2.25	0.076	220.000	0.33

#### 4. NUMERICAL RESULTS

Regarding a consistent analysis for the accuracy of both shear mechanisms, some numerical tests are performed using the butterfly specimen taken hand the material parameters determined based on the calibration procedure above. Three different loading conditions are performance: pure shear ( $0^\circ$ ) and shear/tensile ( $10^\circ$  and  $30^\circ$ ). The performance of some parameters as damage variable, equivalent plastic strain and displacement at fracture as well as the ability to predict the correct fracture onset are evaluated for each loading condition studied.

##### Damage Parameter, Equivalent Plastic Strain and displacement at fracture

The equivalent plastic strain and the displacement at fracture are very important parameters to evaluate the performance and accuracy of the constitutive model as well as the evolution of the damage parameter during all the process. Figure 6 represents the evolution of both damage parameters and equivalent plastic strain at the critical point of the butterfly specimen. Regarding the numerical results for pure shear loading condition (Figure 6a), the GTN model

with Xue's shear mechanism has presented very conservative, predicting the beginning of the failure for a displacement equal to  $u_f = 0.37 \text{ mm}$ , which is in disagreement with the experimental data,  $u_f = 1.03 \text{ mm}$ . Besides that, the GTN model with N&H's shear mechanism and  $k = 1.0$  has presented the best performance, predicting the failure for a displacement near of the experimental data,  $u_f = 0.98 \text{ mm}$ . However, for GTN original model, the failure is not predicted, which is physically inadmissible. In this case, we have only the nucleation of micro crack and the growth mechanism has no ability to capture the behaviour of the material under predominant shear strain.

Then, in the first combined loading condition (shear/tensile :  $10^\circ$ ), see Figure 6b, we have more contribution of the shear loading than the tensile loading, and the Xue's shear mechanism has performance conservative again. But, both shear mechanism predicted the displacement at fracture in disagreement with experimental data. However, for the second combined loading condition (shear/tensile:  $30^\circ$ ), see Figure 6c, the evolution of both mechanisms were very similar. In this case, the contribution of tensile loading, for the damage parameter, is more representative than the contribution of shear loading. Regarding the GTN original model, in the first case, the model predict a large displacement at fracture, and in the second one, the evolution of damage parameter was very similar than the others models. Regarding the evolution of the equivalent plastic strain at fracture, in both cases the parameter presents an evolution very similar. Table 2 contains the numerical and experimental results for both loading conditions.

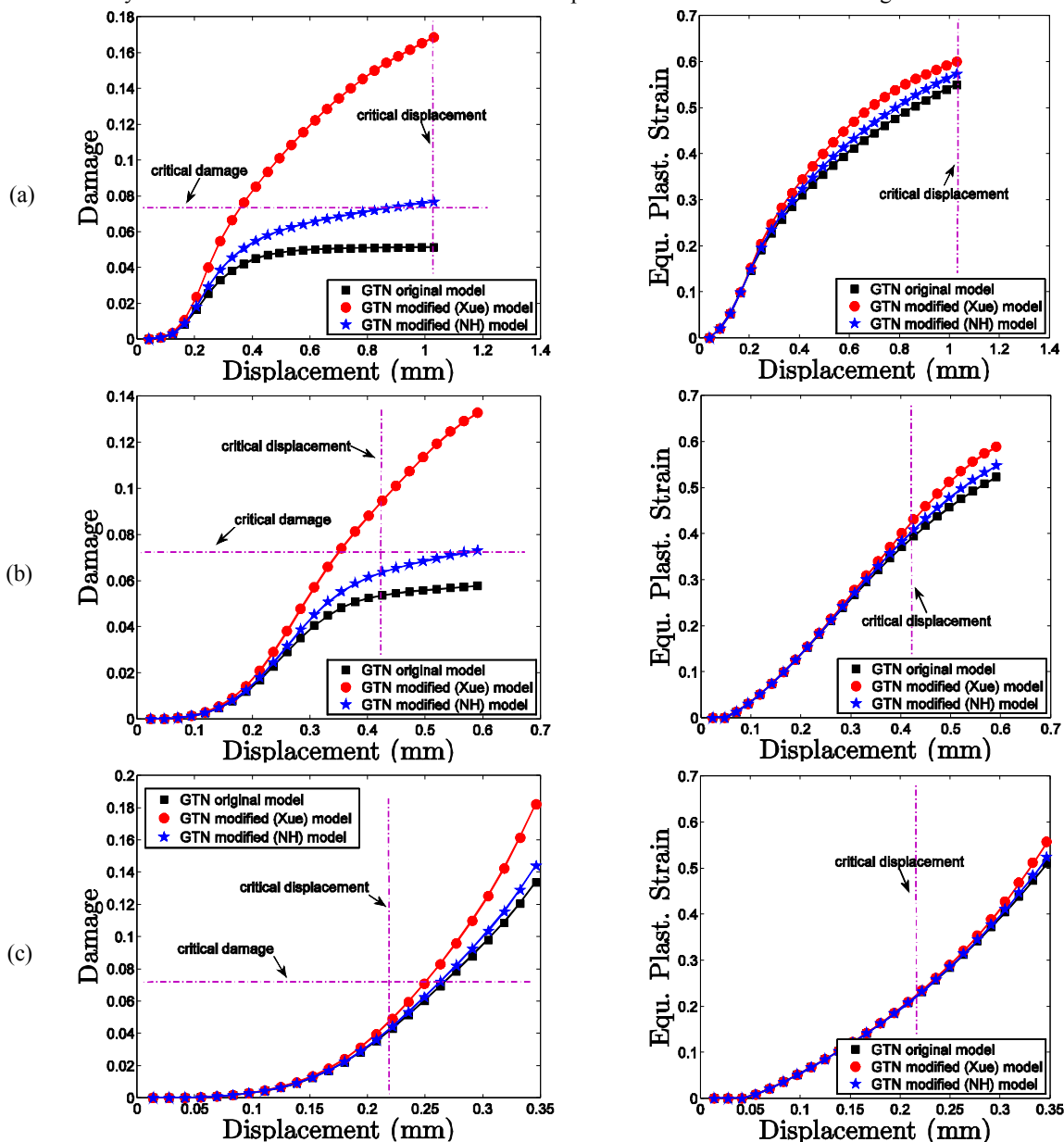


Figure 6. Evolution of the damage parameter and equivalent plastic strain at the critical point.

Table 2: Numerical results for butterfly specimen.

Angle	Experimental data		Numerical results			
	$u_f$	$\bar{\epsilon}^p$		$k$	$u_f$	$\bar{\epsilon}^p$
0°	1.03	0.82	Orig.	---	$\infty$	0.54
			N&H	1.0	0.98	0.58
			Xue	---	0.37	0.32
10°	0.42	0.35	Orig.	---	+1.00	0.52
			N&H	1.0	0.59	0.55
			Xue	---	0.37	0.34
30°	0.22	0.23	Orig.	---	0.16	0.32
			N&H	1.0	0.15	0.32
			Xue	---	0.15	0.32

**Prediction of the fracture onset**

Another important data to be analyzed, regarding the accuracy of both shear mechanism and the GTN original model, is the ability to predict the correct fracture location. Researches as Reis et al. (2010) and Malcher et al. (2010) have shown that the shear mechanisms already proposed in literature, fail in the prediction of the correct location to crack formation when combined loading condition is applied. Based on experimental tests performed by Bai (2008), using the butterfly specimen, it can be observed that in pure shear loading condition, the micro crack is initially formatted in the surface of the critical zone. However, when combined shear/tensile loading condition is applied, the crack is formatted in the middle of the thickness and growth toward the surface of the critical zone. Figure 7 presents the contour of the damage parameter at fracture for both loading conditions. We can conclude that, in pure shear (0°) loading condition, both shear mechanisms have ability to predict the correct site to crack formation. But, for GTN original model, the critical damage parameter is not reached and the parameter is spread around the centre of the specimen. Regarding the first combined loading condition (10°), only GTN model with N&H shear mechanism predicted the correct fracture onset, which is on the central node of the specimen. For the second combined loading condition (30°), both models show the central node, as the potential point to crack initiation, which is in agreement with experimental data.

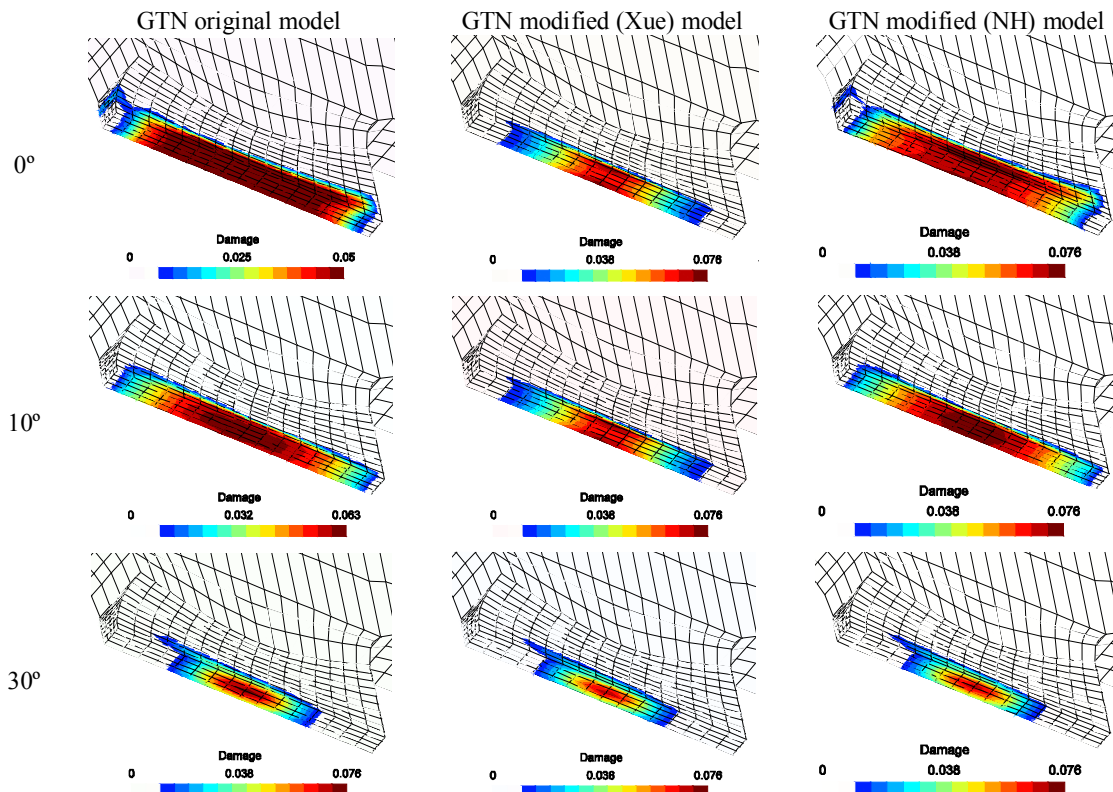


Figure 7. Contour of the damage parameter for both shear mechanisms and GTN original model.

## 5. CONCLUSIONS

In this paper, an assessment of two different shear mechanisms and the GTN original model was performance taken hand the set of material parameters for steel 1045. Numerical results were determined, regarding three different loading conditions, as: pure shear ( $0^\circ$ ) and combined shear/tensile ( $10^\circ$  and  $30^\circ$ ). The evolution of the equivalent plastic strain, the damage parameter and the displacement at fracture were analyzed as well as the ability to predict the correct site to crack initiation. The results have shown that the shear mechanism is a good alternative to improve the GTN model, in order to give ability to use the model under low levels of stress triaxiality. Nevertheless, both mechanisms analysed have presented problems, regarding the prediction of the values for displacement and equivalent plastic strain at fracture, and the potential point to crack initiation. Hence, new improvements need to be developed, in order to give accuracy to the GTN model when predominant shear strain is present.

## 6. ACKNOWLEDGEMENTS

The authors acknowledge the support of Portuguese Science and Technology Foundation (FCT) and the support of University of Brasilia, Faculty UnB at Gama (FGA).

## 7. REFERENCES

- Andrade Pires, F.M., César de Sá, J.M.A., Costa Sousa, L., Natal Jorge, R.M., 2003, Numerical Modeling of ductile plastic damage in bulk metal forming, *International Journal of Mechanical Sciences*, 45:273–294.
- Bai, Y., 2008, Effect of Loading History on Necking and Fracture. Ph.D Thesis, *Massachusetts Institute of Technology*.
- Besson, J., Steglich, D. and Brocks, W., 2001, Modeling of crack growth in round bars and plane strain specimens. *International Journal of Solids and Structures*, 38(46–47):8259–8284.
- Besson, J., 2010, Continuum Models of Ductile Fracture: A Review. *International Journal of Damage Mechanics*, 19:3–52.
- Butcher, C., Chen, Z., Bardelcik, A., Worswick M., 2009, Damage-based finite-element modeling of tube hydroforming. *International Journal of Fracture*, 155:55–65.
- Chaboche, J.L., 1984, Anisotropic Creep Damage in the Framework of Continuum Damage Mechanics. *Nuclear Engineering and Design*, 79: 309–319.
- Chaboche, J.L., 2003, Damage mechanics. In: *Milne, I., Ritchie, R.O. and B. Karihaloo (eds.) Comprehensive Structural Integrity*, vol. 2. Elsevier-Pergamon, pp. 213–284.
- Chaboche, J.L., Boudifa, M., Saanouni, K., 2006, A CDM approach of ductile damage with plastic compressibility. *International Journal of Fracture*, 137:51–75.
- De Souza Neto, E.A., Peri'c, Owen, D.R.J., 2008, Computational methods for plasticity: theory and applications. *John Wiley & Sons Ltd*.
- Engelen, Roy A.B., 2005, Plasticity-induced Damage in Metals / nonlocal modelling at finite strains. PhD Thesis – Eindhoven : Technische Universiteit Eindhoven.
- Gurson, A.L., 1977, Continuum Theory of ductile rupture by void nucleation and growth - Part I. Yield criteria and flow rules for porous ductile media. *J. Engrg. Mat. Tech.*, 99:2-15.
- Krajčini'c, D., Fonseka, G.U., 1981, The Continuous Damage Theory of Brittle Materials – Part 1: General Theory. *J. Appl. Mech.*, 48, 809–815.
- Lemaitre, J., 1985, A continuous damage mechanics model for ductile fracture. *Journal of Engineering Materials and Technology - Trans. of the ASME*, 107:83–89.
- Lemaitre, J., Chaboche, J.L., 1990, *Mechanics of Solid Materials*. Cambridge Univ. Press.
- Malcher, L. ; Andrade Pires, F.M. ; César de Sá, J.M.A., 2011, An Assessment of Isotropic Damage Constitutive Models under High and Low Stress Triaxialities. *International Journal of Plasticity, Submitted for publication*.
- McClintock, F. A., 1968, A Criterion for Ductile Fracture by the Growth of Holes. *J. Appl. Mech.*, 35, 363–371.
- Murakami, S., & Ohno, N., 1981, A Continuum Theory of Creep and Creep Damage. Pages 422–443 of: Ponter, A.R.S. (ed), *Proceedings of the IUTAM Symposium on Creep in Structures*, Leicester, Berlin.
- Nahshon, K., Hutchinson, J., 2008, Modification of the Gurson model for shear failure. *European Journal of Mechanics A/Solids*, 27:1–17.
- Pineau, A., 1981, Review of fracture mechanisms and local approaches to predicting crack resistance in low strength steels. In: François, D. et al. (ed.) *Advances in Fracture Researches*. New-York, Pergamon Press, ICF5. Cannes.
- Reis, F.J.P.; Malcher, L. ; Andrade Pires, F.M. ; César de Sá, J.M.A., 2010, A modified GTN model for the prediction of ductile fracture at low stress triaxialities. *International Journal of Structural Integrity*.
- Rice, J. R., Tracey, D., M., 1969, On the ductile enlargement of voids in triaxial stress fields. *Journal of the Mechanics and Physics of Solids*, 17:201–217.
- Rousselier's, G., 1980, Finite deformation constitutive relations including ductile fracture damage. In: Nemat-Nasser (ed.) *Three-Dimensional Constitutive Relations and Ductile Fracture*. North-Holland Publ. Comp., 1981 pp. 331–

355.

- Rousselier's, G., 1987, Ductile fracture models and their potential in local approach of fracture. *Nuclear Engineering and Design* 105: 97–111.
- Simo, J.C., & Hughes, T.J.R., Computational Inelasticity. New York: Springer-Verlag.
- Teng, X., 2008, Numerical prediction of slant fracture with continuum damage mechanics. *Engineering Fracture Mechanics*, 75:2020–2041.
- Tvergaard, V. and Needleman, A., 1984, Analysis of the cup-cone fracture in a round tensile bar. *Acta Met.* 32:157–169.
- Xue, L., 2007, Ductile Fracture Modeling – Theory, Experimental Investigation and Numerical Verification, Ph.D Thesis, *Massachusetts Inst. of Technology*.